Formulation de milieux et solutions pour les procédés Pharmaceutiques : extrapolation par Computational Fluid Dynamics et validation expérimentale

Régis ANDREUX[1], Miriam AKIKI[1], Guillaume JEANNE[1]

1 : Manufacturing Sciences, Analytics and Technology (MSAT) department, Sanofi, France

Résumé

La fabrication des vaccins et de leurs produits intermédiaires est strictement réglementée et régie par les Directives des autorités sanitaires (European Medicines Agency en 2014). Dans le cadre de son projet EVolutive Facility (EVF) (Sanofi en 2020), Sanofi a mis en place une stratégie de validation de ses milieux et solutions pour assurer leur homogénéité, leur stérilité et leur stabilité. En appui des approches expérimentales traditionnelles, l'utilisation de la Mécanique des Fluides Numérique a été intégrée très tôt dans cette stratégie. La dissolution de poudres en cuve agitée pour la formulation de tampon tréhalose est l'une des composantes de ce plan de validation, pour lequel la vitesse d'agitation et le temps de séjour sont deux paramètres critiques. L'objectif de ce travail est triple : (*i*) une carte phénoménologique des régimes de dissolution est proposée sur la base des rapports des temps caractéristiques qui découlent de la modélisation mécanistique des phénomènes (*ii*) le transfert technologique d'un procédé de dissolution de tréhalose est réalisé en utilisant cette carte et la CFD (*iii*) la stratégie de transfert technologique est validée par une campagne d'essais sur le nouveau système. A l'avenir, cette méthodologie sera appliquée à nos autres procédés**.**

Formulation of media and solutions for Pharmaceutical processes: extrapolation by Computational Fluid Dynamics and experimental validation

Régis ANDREUX[1], Miriam AKIKI[1], Guillaume JEANNE[1]

1 : Manufacturing Sciences, Analytics and Technology (MSAT) department, Sanofi, France

Abstract

The manufacture of vaccines and their intermediate products is strictly regulated and governed by the Guidelines of the health authorities (European Medicines Agency in 2014). As part of its EVolutive Facility (EVF) project (Sanofi in 2020), Sanofi has implemented a validation plan strategy for its media and solutions to ensure their homogeneity, sterility, and stability. In support of traditional experimental approaches, the use of Computational Fluid Dynamics (CFD) was incorporated early in this strategy. Powder dissolution in a stirred tank for the formulation of an osmolyte is one of the components of this validation plan, for which the stirring speed and residence time are two critical parameters. The objective of this work is threefold: (*i*) a novel phenomenological mapping of the dissolution regimes is build based on ratios of the characteristic times that derives from mechanistical modelings (*ii*) the technology transfer of an existing dissolution process is performed using this map and Computational Fluid dynamics (*iii*) the technology transfer strategy is validated comparing to experimental campaign on the new process. Further work will allow us to deploy the methodology to all our media buffer preparation.

1. Introduction, motivation, and strategy

Powder dissolution flows are encountered in a wide range of unit operations dedicated to the vaccine Up-Stream and Down-Stream Processes (USP, DSP) for organic osmolytes preparation (Yancey in 2005). At industrial scales, stirred tanks are usually used to manufacture buffers that have volumes of dozens to thousands of liters, in close-to saturation conditions. Because of reglementary Good Manufacturing Practices reasons and the historical evolution of production sites, a buffer is sometimes manufactured in reactors with many different sizes and designs. Technology transfer with scale-up and scale-down problematics is thus standard work. Up to now, it has been based on technical know-how and trial-error methods to assess the Normal Operating Conditions (NORs) and the Proven Acceptable Ranges (PARs) required by the Guidelines of the health authorities.

Today, with the emergence of multiple single-use technologies (Shukla in 2013, Langer in 2022) and the need to reduce time-to-market of future vaccines (Pollard in 2021), modeling studies have become a complementary *must-have*. Computational Fluid Dynamics (CFD), by its ability to describe the hydrodynamics, counting for eventual unconventional designs of stirred tanks, is an efficient tool for such a work (Pohar in 2020, Sommer in 2021, Thomas in 2021, Pordal in 2022, Murthy in 2008, Grisafi in 2023, Kersebaum in 2024).

Sanofi has a large amount of R&D and production sites over the world, potentially leading to hundreds of variations of stirred tank technologies dedicated to buffer preparation. Considering also the computational time required to simulate industrial-sized polyphasic reactors (Shu in 2018, Neau in 2020), the blind and unlimited use of CFD is unthinkable. Thus, a goal for Sanofi is to pragmatically rationalize and simplify its use.

The purpose of the current work is (*i*) to build a phenomenological methodology to determine whether CFD is absolutely required for the technology transfer of a dissolution process. It is based on the micro-scale characteristic times of each phenomenon that are involved (*ii*) to follow this methodology to perform the technology transfer of a dissolution unit operation, using CFD implemented in the M-Star commercial code, v3.8.77 (*iii*) to validate the methodology with an experimental investigation on the new vessel, using visual observation and chromatography measurements (HPLC).

Our usage case is the dissolution of trehalose (Rowe in 2009). In biological chemistry, trehalose is a well-known osmolyte used as an efficient protective agent (Arakawa in 1982, Crowe in 1992, Leslie in 1995, Richards in 2002, Kaushik in 2003) in various unit operation such as viral filtration (Wickramasighe in 2019). The trehalose concentration is arbitrarily set to 40% in this study.

In a first section, we recall the theory of mechanistical modeling of dissolution, to present the macro-scale and micro-scale characteristic times on which our study is based. We propose a new mapping of dissolution regimes based on the micro-scale characteristic times. We quickly recall the theory and equations of CFD.

In second section, we use the novel mapping combined with the CFD to investigate the trehalose dissolution in an industrial stainless-steel vessel.

In a third section, we perform the technology transfer of the trehalose dissolution to a single-use stirred tank. An evaluation of the cost reduction achieved using modeling is conducted.

Finally, the conclusion summarizes the main results and presents the perspectives of this work.

2. Mathematical and mechanistic modeling

Overview of the powder dissolution mechanisms

The dissolution of an isolated solid particle immersed in a moving fluid stirred in a vessel is driven by four competing physical phenomena:

- The solvation step (Grijseels in 1981): the surface reaction of the particle loses individual molecules that accumulate in the liquid phase at the fluid-particle interface. It is driven by thermodynamics considerations. In most cases, this mechanism could be considered instantaneous and not limit the dissolution process.
- The particle-to-liquid diffusive mass transfer, *i.e.* the diffusive transport of dissolved molecules from the fluid-particle interface into the bulk fluid solution. It is driven by local solute concentrations and local fluid-particle hydrodynamics coupling. In most cases, this mechanism is limiting, so that dissolutions in liquids could be considered diffusion-controlled (Cartensen in 1972).
- The macroscopic fluid mixing, *i.e.* the convective transport of these dissolved molecules in the vessel. It is driven by the design space. This mechanism could be limiting, for example, when local over- or under-solute concentrations are observed because of a low fluid mixing. See Paul in 2003, for a complete description of mixing effects in industrial processes.
- - The macroscopic particle mixing, *i.e.* the results of the competition between the transport due to fluid entrainment and the particle settling due to gravity. This mechanism could be limiting, for example when the particles float on the surface of the liquid or settle in the bottom of the stirred tank (Hemrajani in 2003).

Macro-scale characteristic times

It is convenient to define several time scales to characterize the dissolution of particulate flows. Usually, the Chemical Engineering approach tends to consider macroscopic times scales:

- The macro-scale characteristic time of fluid mixing in a vessel. It is the time required to reach 95% of homogeneity in the whole vessel after a fluid perturbation, τ_{95}^{Mix}.
- The sedimentation time of the particles in the vessel.
- The macro-scale characteristic time of particle dissolution. It equals the time required for an isolated particle surrounded by perfectly mixed fluid to be completely dissolved, τ_{M}^{D}.

However, macro-scale characteristic times do not represent intrinsic phenomena since there are the results of the overall process. Thus, we propose to use the micro-scale characteristic times to establish a new mapping of dissolution regimes.

Micro-scale characteristic times

Particle solvation

Assuming that this mechanism is instantaneous, the micro-scale characterization time will be considered zero.

Particle-to-liquid diffusive mass transfer : τ_{12}^{D}

The solute flux J at the solid-liquid interface during the dissolution of an isolated particle can be expressed as

$$J = k_c(C_i - C) \qquad (1)$$

where J, k_c, C_i and C imply the local solute flux leaving the particle interface, the fluid-particle mass transfer coefficient, the solute volumetric concentration at the particle-liquid interface, and that in the bulk of the solution, respectively. It is commonly stated C_i and the solute volumetric concentration at saturation are equal. Thereby, C_i will be replaced with C_{sat} in the followings.

Assuming perfect fluid and particle mixings, and neglecting potential particle-particle interactions, the volumetric integration of Eq. (1) over the whole vessel leads to the global mass balance equation of the dissolved solute:

$$\mathcal{V}_f \frac{\partial C}{\partial t} = k_c \mathcal{S}_p (C_{sat} - C) \quad (2)$$

Where $\mathcal{V}_f$ is the liquid volume in the vessel and $\mathcal{S}_p$ is the total particle surface area exposed to the liquid. Mathematical manipulation of Eq.(2) leads to

$$\frac{\partial C}{\partial t} = k_c \frac{1}{\rho_p d_p} \frac{\phi_{p\varsigma}}{\phi_{pv}} (C^* - C) (C_{sat} - C) \quad (3)$$

Where C^*, ρ_p and d_p are the solute volumetric concentration for total solid dissolution, the particle density and diameter, respectively.

$\phi_{p\varsigma}$ represents the surface shape factor that is a coefficient of the particle surface area ς_p , which can be expressed as a quadratic function of d_p:

$$\varsigma_p = \phi_{p\varsigma} {d_p}^2 \quad (4)$$

ϕ_{pv} represents the volume shape factor that is a coefficient of the particle volume υ_p, which can be expressed as a cubic function of d_p:

$$\upsilon_p = \phi_{pv} {d_p}^3 \quad (5)$$

Finally, the extent of the dissolution χ is given as follows:

$$\chi = \frac{C - C_0}{C^* - C_0} \quad (6)$$

where C_0 the initial value of C in the liquid.

As proposed by Froessling in 1958 and consistently with the Ranz-Marzhall's correlation, in 1952, for heat transfer, the fluid-particle mass transfer coefficient k_c of an isolated particle in a surrounding flowing fluid is often given by Eq.(7)

$$k_c = \mathcal{D} {d_p}^{-1} \left(2.0 + 0.6 {Re_p}^{1/2} {S_c}^{0.3}\right) \quad (7)$$

where $\mathcal{D}$ is the fluid phase molar diffusion coefficient, S_c is the Schmidt number defined as $S_c = \frac{\mu_F}{\rho_F \mathcal{D}}$, and $Re_p = \frac{\rho_F |\boldsymbol{V_r}| d_p}{\mu_F}$ is the particle Reynolds number. ρ_F and μ_F are the fluid density and dynamic viscosity, respectively. The determination of Re_p requires the knowledge of the slip velocity $\boldsymbol{V_r}$ between the particle and the fluid phases.

Mathematical manipulation of Eq. (3) leads to:

$$\frac{\partial C}{\partial t} = (\tau_{12}^D)^{-1} (C_{sat} - C) \quad (8)$$

with τ_{12}^D, the characteristic time of local particle dissolution:

$$(\tau_{12}^D)^{-1} = k_c \frac{1}{\rho_p d_p} \frac{\phi_{p\varsigma}}{\phi_{pv}} (C^* - C) \quad (9)$$

Eq. (3) is solved using the fourth order Runge-Kutta method, with the following initial condition: $C_{@t=0} = 0$.

Fluid mixing : τ_1^{Mix}

The micro-scale characteristic time of fluid mixing is not usually considered and has never been discussed in the literature. Assuming a mathematical isomorphism with the dissolution equation Eq. (8), we suggest the following equation:

$$\frac{\partial \Delta C_{95\%}}{\partial t} = \left(\tau_1^{Mix}\right)^{-1}(1 - \Delta C_{95\%}) \quad (10)$$

where $\Delta C_{95\%}$ is the volumetric ratio of fluid that has reached 95% of homogeneity in the vessel at time t.

Particle sedimentation : τ_{12}^{F}

The forces that apply to each particle are supposed to be reduced to fluid-particle drag force, buoyancy force, and gravity force.

Assuming that the particles and fluid are in a state of hydrodynamic equilibrium, the resulting force balance equation for each particle is:

$$F_d = F_g \quad (11)$$

Where F_g, sum of gravity and buoyancy contributions, is given by:

$$F_g = g(\rho_P - \rho_F)V_P \quad (12)$$

And the drag force, F_d, is given by:

$$F_d = (\tau_{12}^{F})^{-1}|\boldsymbol{V_r}|\,\rho_p \quad (13)$$

With the slip velocity V_r between the particle and the fluid. τ_{12}^{F}, the characteristic time of local particle entrainment by the fluid motion or particle relaxation time, relates to inertial effects acting on the particles due to the drag force (Simonin in 1991):

$$\tau_{12}^{F} = \left(\frac{3}{4}\frac{\rho_1}{\rho_2}\frac{|\boldsymbol{V_r}|}{d_p}C_d\right)^{-1} \quad (14)$$

C_d is the drag coefficient, given by the Schiller-Naumann's correlation (Naumann in 1935):

$$C_d = \frac{24}{Re_p}\left(1 + 0.15Re_p^{0.687}\right), for\ Re_p < 10^3 \quad (15)$$

The Generalized Reduced Gradient (GRG) method (Lasdon in 1974) can be used to solve the non-linear system of Eq. (11) - (15) for the determination of τ_{12}^{F} and $|\boldsymbol{V_r}|$.

Mapping of the dissolution regimes and impact on the tech-transfer strategy

The new mapping of the dissolution regime we propose is presented in Figure 1. It is based on ratios between the micro-scale characteristic times established for an isolated particle in the stirred vessel (i.e. considering the fluid properties as constant).

Seven regimes of dissolution are found:

- The fully coupled regime (noted 01 in Figure 1): fluid mixing, particle mixing, particle-to-liquid mass diffusion are in competition. The dissolution process may be very sensitive to the design of the stirred tank and its impeller, and all operating parameters (*e.g.* impeller rotation speed, liquid working volume, residence time) can be critical to product specifications. CFD based on the modeling of all the physical mechanisms involved, should be used for the investigation of such systems.

- The first asymptotic dissolution regime, driven by the dominant limiting mechanism of particle mixing (noted 04 in Figure 1). The drag force exerted by the fluid on the particles in not sufficient and they therefore float on the surface of the liquid or settle at the bottom of the vessel. Hydrodynamics CFD should be used for the investigation of such systems.
- The second asymptotic dissolution regime, driven by the dominant limiting mechanism of fluid mixing (noted 03 in Figure 1). The force exerted by the impeller on the fluid is not sufficient to homogenize the concentration of solute. Over- and under- concentrated fluid zones can be observed, and resulting local oversaturation can be observed. Hydrodynamics CFD should be used for the investigation of such systems.
- The third asymptotic dissolution regime, driven by the dominant limiting mechanism of particle-to-fluid mass diffusion (noted 02 in Figure 1). Eq. (8) and Eq. (9) show that this regime can occur for two reasons: (*i*) due to a decrease in the local slip velocity between particles and fluid, $\boldsymbol{V_r}$, when particles become smaller and smaller, or when the fluid viscosity increases (*ii*) due to increase in the extent of dissolution, especially when the final product is close to saturation. Hydrodynamics CFD could eventually be used for the investigation of such systems.
- Partially coupled regimes (noted 05, 06, 07 in Figure 1), which are driven by two of the three limiting mechanisms.

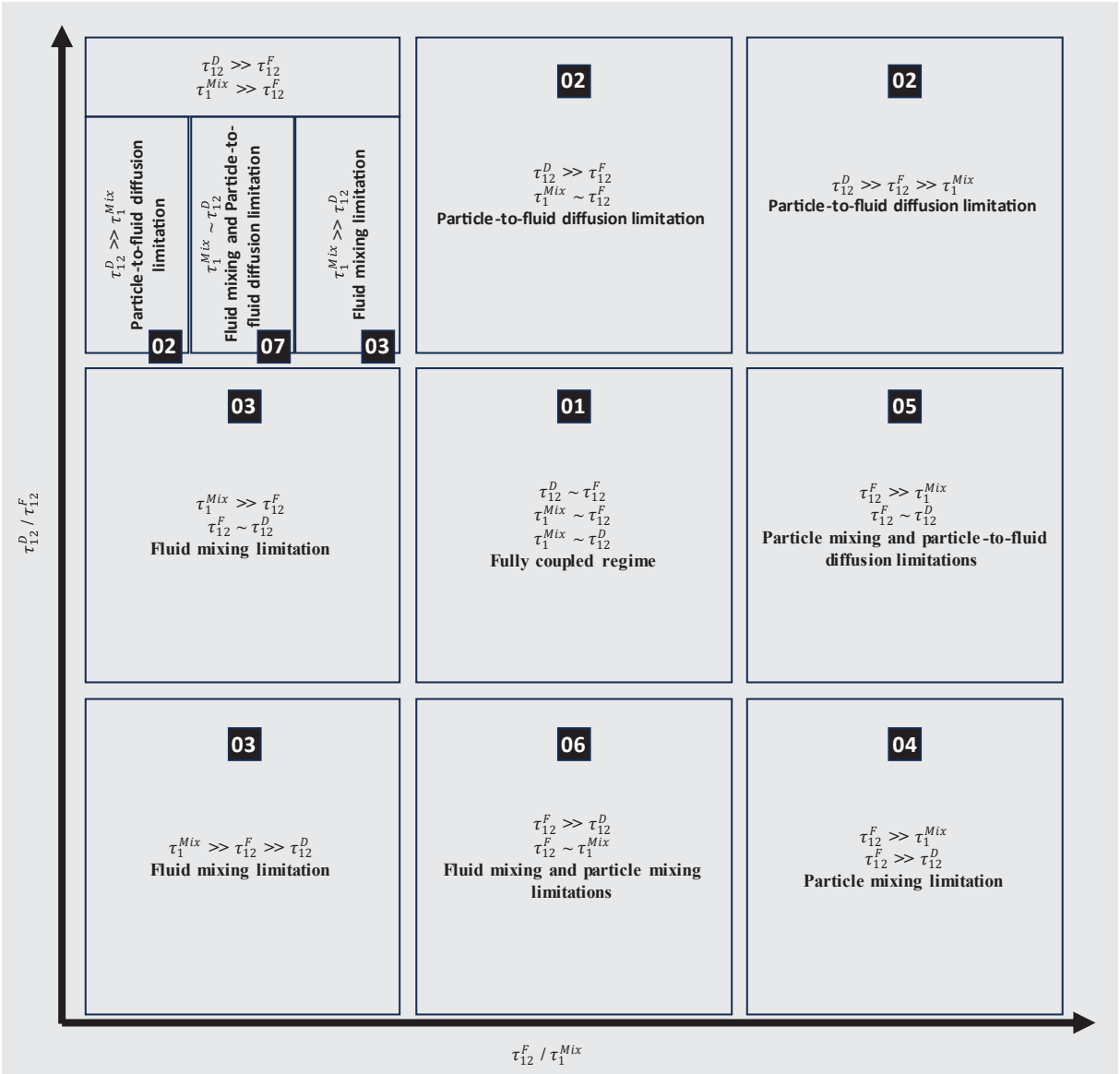

Figure 1. Mapping of the dissolution regime

Computational Fluid Dynamics theory

The commercial CFD code M-Star (v.3.8.77) developed by M-Star Simulation LLC was used to simulate the hydrodynamics of stirred tanks.

Fluid hydrodynamics modeling

The CFD code is based on the Lattice-Boltzmann Method approach to solving transient Navier-Stokes equations. A D3Q19 lattice is used. Turbulence effects are counted in the frame of the Smagorinsky-Lilly sub-grid closure model (Smagorinsky in 1963). The free surface phenomenon is counted using the Volume of Fluid (VoF) method in order to track the shape of the gas-liquid interface that separates the gaseous sky from the stirred liquid (Hirt in 1981). Refer to Kersebaum in 2024 and the M-Star technical documentation for more details.

Fluid tracer propagation modeling

Fluid mixing is investigated introducing a passive scalar convected by the fluid phase. The corresponding transport equation is:

$$\frac{\partial \alpha}{\partial t} + \nabla \boldsymbol{U} \alpha = 0 \qquad (16)$$

Where α is the volumetric concentration of the species, $\boldsymbol{U}$ the fluid local velocity. A second order Van Leer spatial discretization is used on convection term to prevent from non-physical numerical diffusion of the tracer.

Computational parameters

Following the recommendations of the Supporting Information for Kersebaum's article in 2024, a uniform cartesian grid with between 200 and 300 points across the diameter of the tank is a good compromise between performance and accuracy. Therefore, we choose a grid with 250 points. The time step is set constant, calculated based on a maximum Courant number of 0.05. Two preliminary simulations of a few seconds of physical time, considering 200 points and 300 points, confirm an effect of less than 5% on the results, based on the calculation of the mechanical energy transmitted to the fluid by the rotating impeller. The fluid properties are considered constant throughout the duration of each simulation.

3. Application: trehalose buffer preparation in an existing stirred tank

Experimental set-up

The dissolution of trehalose is conducted in a batch: a stirred vessel was filled with water. At zero time, a known amount of solid particles was poured into the vessel.

The industrial-sized device is a stainless-steel vessel with a working volume of 0.120 m^3 (Figure 2) and a heigh-to-diameter ratio of 1.5. A GMP impeller rotating around a decentralized axis with a rotating speed of $\dot{\phi}_0$ is used. The ratio of the vessel diameter to the impeller diameter is 5. The system is known to perform qualified dissolution at a range of the impeller rotation speed of +/- 10%.

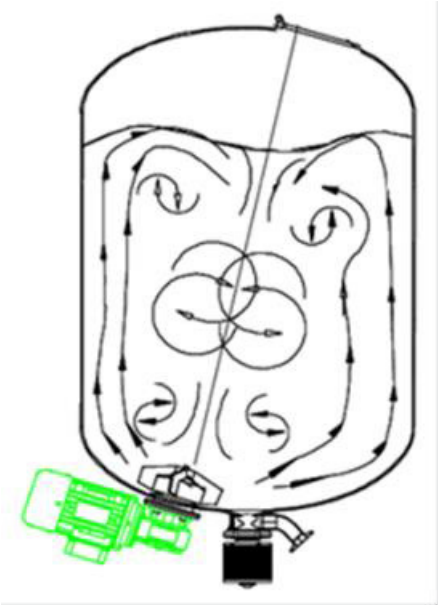

Figure 2. Presentation of the existing stirred tank and its impeller

The vessel is initially filled with water, with a density of 1000 kg.m^{-3}, and a dynamic viscosity of 10^{-3} Pa.s.

The powder consists of poly-dispersed particles of trehalose. Behavior is summarized in Tableau 1. Less trehalose than is needed to attain the saturation was initially poured into the system (C^*=442 kg.m^{-3}, C_{sat}=689 kg.m^{-3}).

Tableau 1. Power behavior of VPB preparation.

Chemical	**Water Solubility** **g.L^{-1} @ 20°C**	**Bulk density** **kg.m^{-3}**	**Quantity** **kg**	**Granulometry** **µm**	**Molar mass** **g.mol^{-1}**
Trehalose	689	600	287	950	378.33

Investigation

Characterization times and consequent dissolution regime

The extent of dissolution over time of an isolated particle surrounded by perfectly mixed fluid is presented in Figure 3. It is obtained solving Eq. (8). The overall dissolution process is carried out in 150 seconds (τ_{M}^{D} = 150 s).

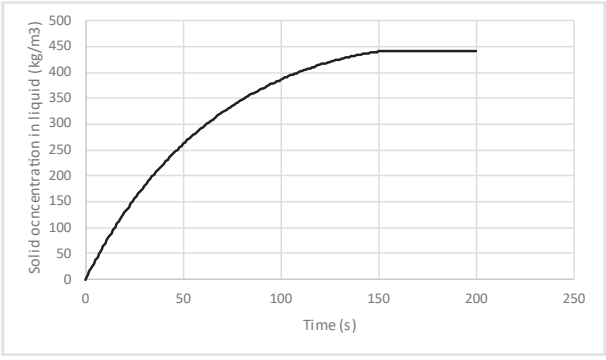

Figure 3. Extent of dissolution over time for an isolated particle surrounded by perfectly mixed fluid – Simulation

The micro-scale characteristic time of the dissolution, τ_{12}^{D}, calculated with Eq. (9), equals hundred at the beginning of the dissolution and increases exponentially (Figure 4). This trend is explained as follows: particle size decreases with the advancement of dissolution, leading to a decrease in diffusive transfer. Theoretically, when the particles are infinitely small, the diffusive transfer is zero, and characteristic time tends towards infinity.

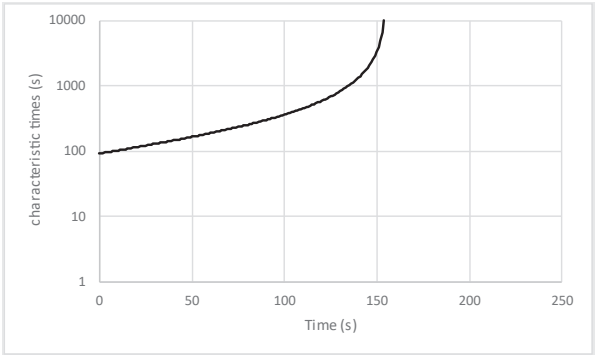

Figure 4. Micro-scale characteristic time of the dissolution along time for an isolated particle surrounded by perfectly mixed fluid – Simulation

The particle relaxation time, τ_{12}^{F}, is calculated using Eq. (14), assuming a constant density and viscosity of the fluid during dissolution, even if this is not rigorously true. τ_{12}^{F} decreases continuously during the dissolution process and is always less than 22 milliseconds (Figure 5). As before, the decrease in particle size with the advancement of dissolution explains this trend. Theoretically, when the particles are infinitely small, τ_{12}^{F} tends towards zero and the particles follow the fluid perfectly

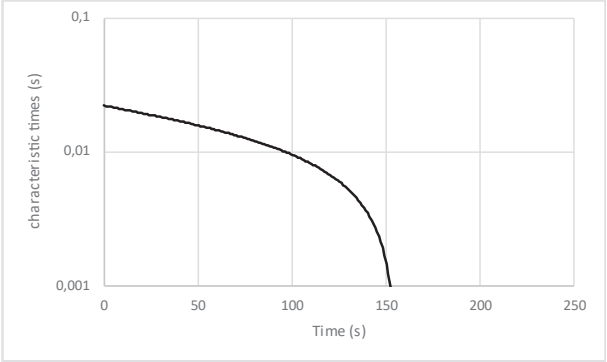

Figure 5. Particle relaxation time along the dissolution. Simulation

The fluid macro-scale mixing time, τ_{95}^{Mix}, is evaluated using Computational Fluid Dynamics. The fluid flow is simulated under conditions prior to the powder spill. Once the flow is fully developed, a thin layer of fluid is traced in the upper zone of the stirred tank with a passive scalar and the tracer propagation is investigated.

Simulations show that the fluid mixing is very effective (Figure 6). The rotation of the impeller creates a downward suction movement of the fluid at the center of the tank, with dispersion at the bottom and the liquid rising along the walls.

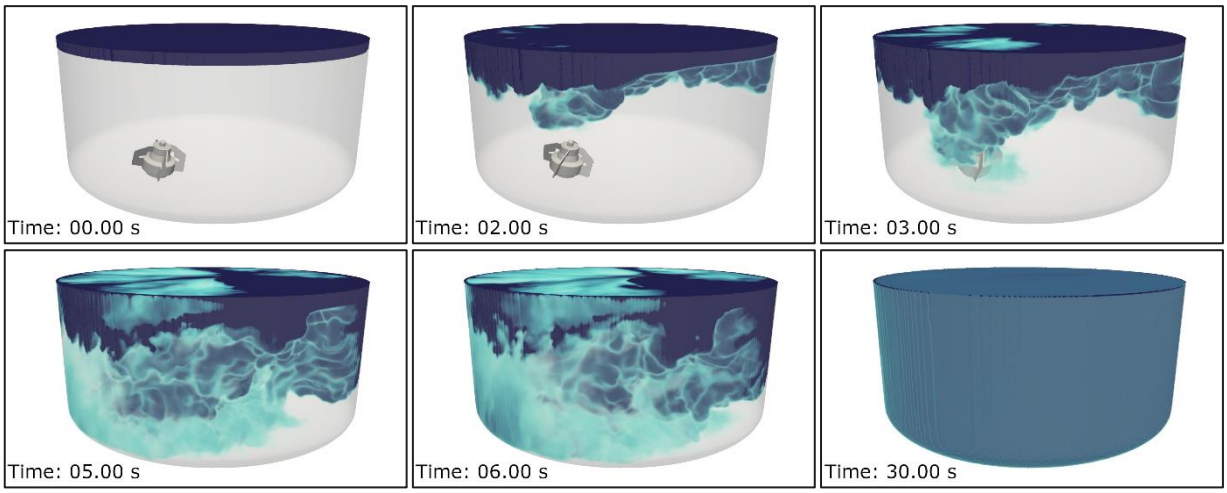

Figure 6. Fluid tracing in the existing vessel

The plot of the proportion of volume that has reached 95% of the final concentration value is given in Figure 7. The macro-scale characteristic time of fluid mixing, τ_{95}^{Mix}, *i.e.* the time at which the 100% value is reached, equals 30 seconds. Retro-fitting calculation based on Figure 7 and Eq. (10), shows that the micro-scale characteristic time of fluid mixing, τ_{1}^{Mix}, ranges between one and forty seconds during the mixing process (Figure 7-right).

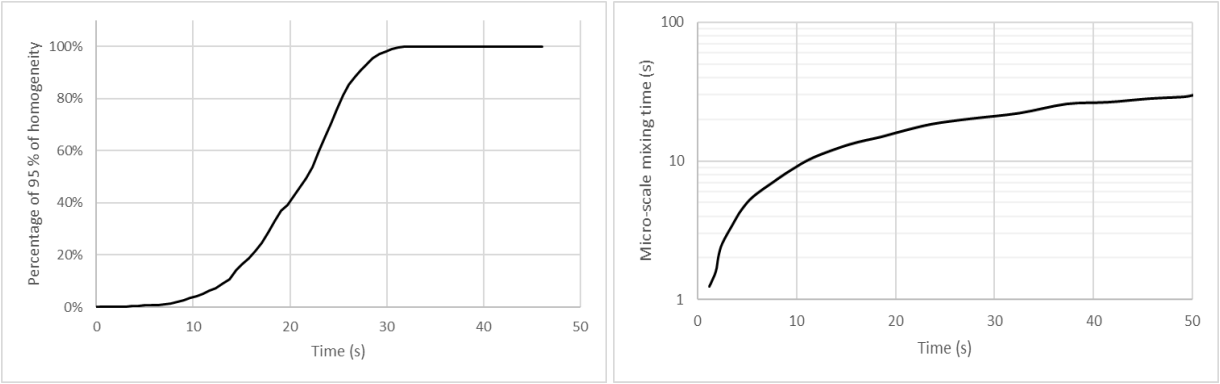

Figure 7. Evolution of the volumetric percentage of the fluid in the existing stirred tank that has reached 95% of homogeneity after fluid tracer injection - CFD simulation (left). Micro-scale characteristic time of the fluid mixing in the stirred tank along time after fluid tracer injection – retro-fitting (right)

Following Figs. (4)(5)(8), $\tau_{12}^{D} >> \tau_{1}^{Mix} >> \tau_{12}^{F}$. The dissolution process carried out under these conditions therefore belongs to the third asymptotic dissolution regime, driven by the dominant limiting mechanism of particle-to-fluid mass diffusion (noted 02 in Figure 1).

4. Application: tech-transfer of the trehalose buffer preparation

Experimental set-up

We are considering the same powder and fluid and experimental protocol as in the previous vessel. The dissolution is now carried out in a single-use vessel with a working volume of 0.200 m^3 (Figure 8) and a height-to-hydraulic diameter of 1. A centered-axis turbine is used. The ratio of the vessel hydraulic diameter to the impeller diameter is 3.75.

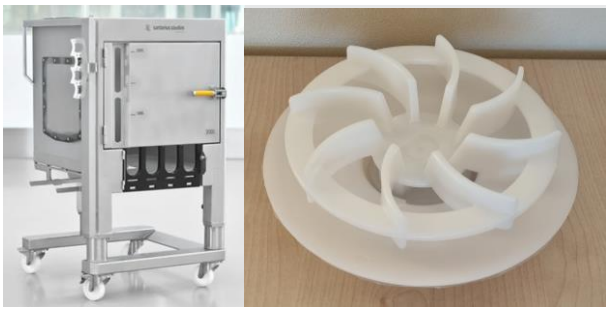

Figure 8. Presentation of the single-use stirred tank (Promixer Sartorius)

Preliminary considerations on technology transfer and strategy

The numerical approach is used to determine the rotation speed of the impeller that mimics the dissolution process studied previously.

If the goal of the current study was to optimize the existing dissolution process, we would logically have investigated the increase of limited mechanism, *i. e.* the particle-to-fluid mass diffusion. See Mishra, in 2020, for a review of factors influencing liquid-solid suspension behavior in stirred tanks.

However, the goal of our study is not to do this. Rather, it is to transfer the current process to a new technology of stirred tank, minimizing efforts and risks, and time-to-market. Thus, our strategy must consist of mimicking the fluid and particles mixings and the particle-to-fluid mass diffusion in the future stirred tank with their eventual limitations.

Since fluid and particles are identical in both stirred tanks, and following Eq.(3) and Eq. (7) and Eq. (11)-(15), τ_{12}^{D} and τ_{12}^{F} are kept constant. The effort should be focused on respecting the fluid mixing by adjusting the rotation speed of the impeller.

Determination of the impeller rotation speed

The influence of the rotation speed of the impeller on the macro-scale characteristic time of the fluid mixing, τ_{95}^{Mix}, is presented in Figure 9. The rotation speed of the impeller of the future stirred tank should be 80% higher than that of existing stirred tank to reproduce the fluid mixing: $\dot{\phi} = 1.8\ \dot{\phi}_0$.

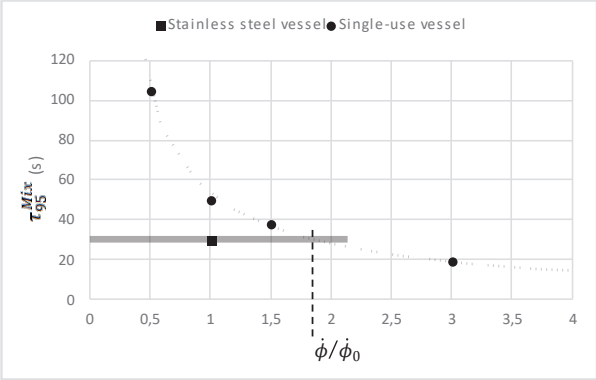

Figure 9. Effect of the impeller rotation speed on the macro-scale characteristic time of fluid mixing in the new stirred tank. Visualization of the optimum value to ensure the technology transfer

At this operating condition, the fluid tracer propagation visualization suggests that the fluid mixing is as efficient as in the existing stirred tank (Figure 10).

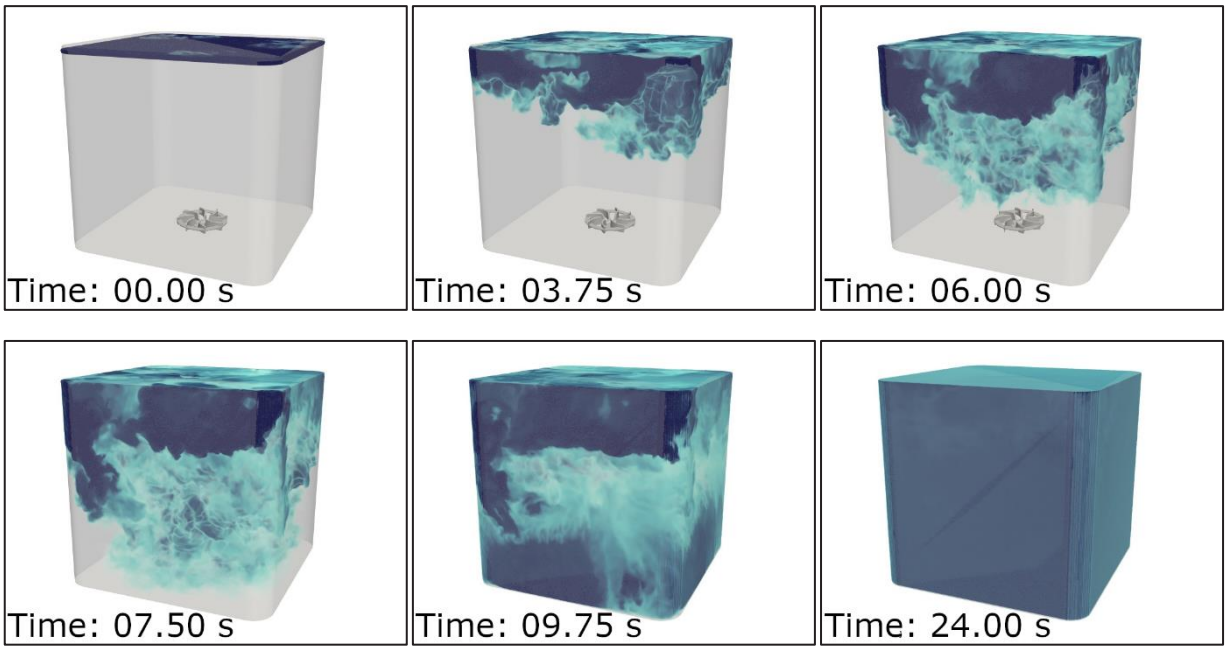

Figure 10. Fluid tracing in the new vessel

Retro-fitting calculation leads to micro-scale characteristic time of fluid mixing, τ_1^{Mix}, similar to that of the existing system (Figure 11).

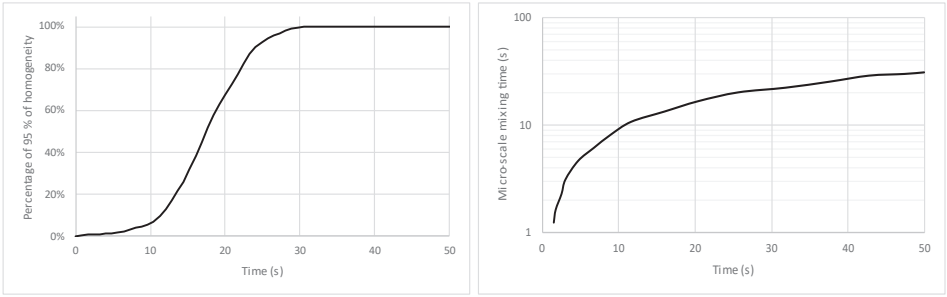

Figure 11. Evolution of the volumetric percentage of the fluid in the new stirred tank that has reach 95% of homogeneity after fluid tracer injection - CFD simulation (left). Micro-scale characteristic time of the fluid mixing in the stirred tank along time after fluid tracer injection – retro-fitting (right)

Assessment of extra-data using CFD

Fluid turbulence is sometimes considered critical in pharmaceutical processes (Croughan in 2006, Merten in 2015). The size of the smallest turbulent eddies in fluid flows, *i.e.* the spatial Kolmogorov length scale (Kolmogorov in 1941), is usually studied when a process is investigated.

CFD simulation provides the probability density functions of the spatial Kolmogorov length scales. The curves, non-dimensionalized by their mean values, are presented in Figure 12. The two curves are very similar, and well-approximated by a log-normal law. Note that the design of the new impeller produces a slightly more spread-out range of Kolmogorov length scale.

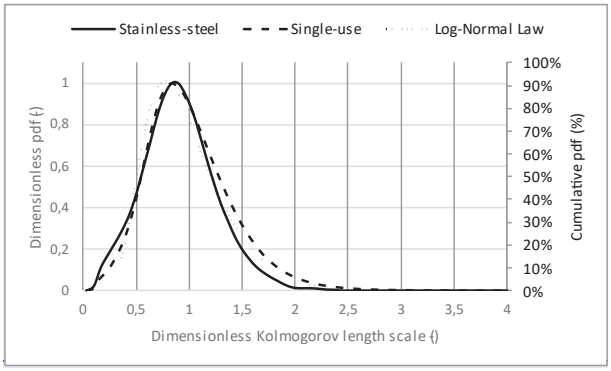

Figure 12. CFD prediction of the probability density function of the dimensionless Kolmogorov length scales in the existing and in the single-use vessels

Experimental validation

The extent of dissolution over time was experimentally studied by visual observation, and solute trehalose dosing measured with off-line HPLC. Four sampling points were used: at the central point of the vessel at three elevations (10%, 50% and 90% of the fluid surface level), and at the wall at an elevation of 90% of the fluid surface level (Figure 13). The sampling are made at T0, T0 + 5 min, T0 + 10 min, T0 + 15 min, T0 + 30 min, T0 + 60 min. Due to our industrial protocol, T0 corresponds to the time at which the powder is poured into the liquid plus a minute. Two impeller rotation speeds were tested: target speed, and 80% of target speed.

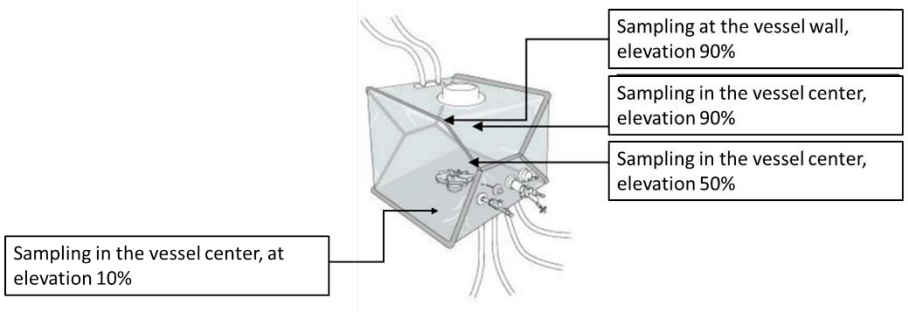

Figure 13. Position of the four sampling points for solute trehalose dosing using off-line HPLC

At 80% of the target speed, the dissolution process is ineffective: the powder is settling at the bottom of the vessel, and small powder aggregates are always observed (Figure 14).

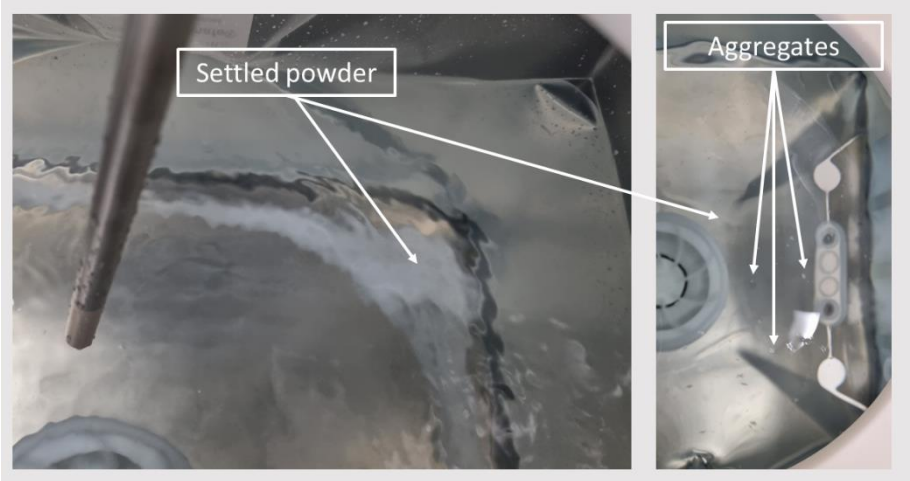

Figure 14. Experimental visualization of particles settling and aggregates formation at 80% of target speed

At 100% of the target speed, visual observations suggest the effectiveness of the dissolution process (Figure 15).

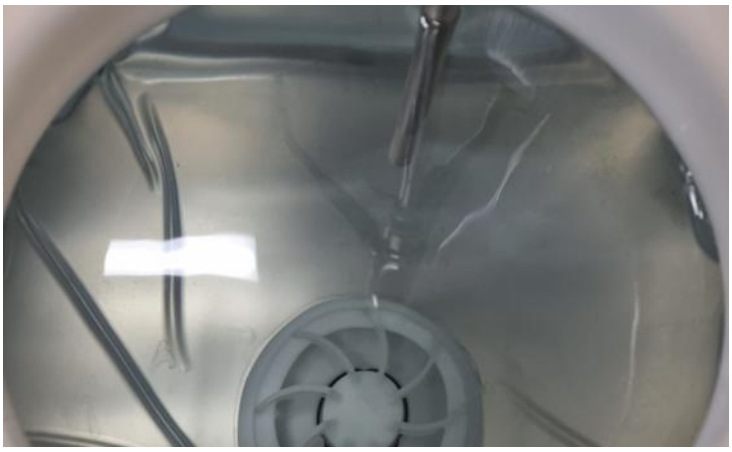

Figure 15. Experimental visualization of the dissolution process accuracy at target speed

Moreover, the concentrations of trehalose solute measured over time at the different sampling points confirm that the dissolution process is rapid (Figure 16): at T0, the concentration has almost reached its final value. They also confirm the efficiency of the fluid mixing since the measured values are equal at any sampling point to the measurement uncertainty.

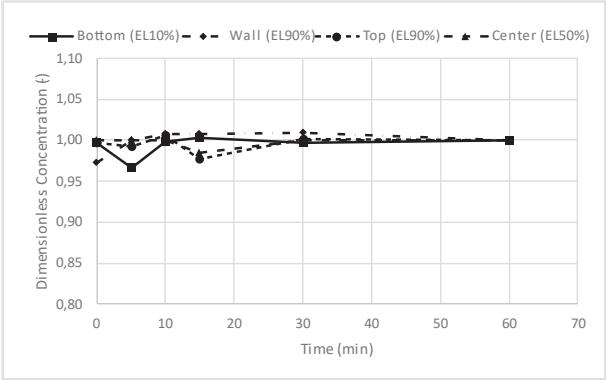

Figure 16. Dimensionless concentration of the solute trehalose measured at the four sample points with offline HPLC along the time at target speed

Cost reduction evaluation thanks to CFD

The cost reduction to determine the optimum rotation speed of the impeller in the future technology of stirred tank is estimated at 55% on CAPEX (single-use bags, batches of liquids and powders, measurement campaigns with HPLC). In addition, a 50% reduction in FTEs has redirected human resources towards higher value-added tasks to accelerate the development of other protocols related to our product during technology transfer. The time required to determine the final rotation speed of the impeller in the new single-use vessel has been divided by a factor of two.

5. Conclusions

A new mapping of the dissolution regimes is proposed, based on the micro-scale characteristic times of the physical mechanisms involved in the dissolution of powders, including fluid mixing, particle mixing, and particle-to-fluid mass diffusion. It identifies limiting mechanisms in a dissolution process, and therefore helps define the modeing strategy for technology transfer.

The methodology is applied to the technology transfer of one of Sanofi's industrial processes, *i.e.* the preparation of a solution of trehalose in a stirred tank. We show that the existing process is limited by the particle-to-fluid mass diffusion.

In order to minimise efforts and risks as well as time-to-market, we combined the proposed approach with CFD simulation to carry out the transfer of technology to a new single-use stirred tank. The new dissolution process is found to successfully work under exactly the same dissolution conditions as the existing process.

Experimental validation was performed on the device, by visual observation and HPLC offline measurements. The new process was shown to be effective, and the Proof of Concept of the technology transfer method was a success. Further work will focus on deploying this methodology to other Sanofi processes involving buffer preparation.

This work was funded by Sanofi.

All authors are Sanofi employees and may hold shares and/or stock options in the company.

Références bibliographiques

Arakawa, T. & Timasheff, S. N., 1982, Stabilization of protein structure by sugars. *Biochemistry* 21, :36–6544.

Cartensen, J. T., 1972, Theory of pharmaceutical systems. *IAcademic Press, New-York* 219–241.

Croughan, M. S., Hamel, J. & Wang, D. I. C., 2006, Hydrodynamic effects on animal cells grown in microcarrier cultures. *Biotechnol. Bioeng.* 95:295–305.

Crowe, J. H., Hoekstra, F. A. & Crowe, L. M., 1992, Anhydrobiosis. *Annu. Rev. Physiol.* 54:579–599.

European Medicines Agency, 2014, ICH Q8 (R2) Pharmaceutical development - Scientific guideline. *EMA/CHMP/ICH/167068/2004*.

Froessling, N., 1958, Evaporation, heat transfer, and velocity distribution in two-dimensional and rotationally symmetrical laminar boundary layer flow. *National Advisory Committee for Aeronautics - Technical Momorandum 1432*.

Grijseels, H., Crommelin, D. J. A. & Blaey, C. J., 1981, Hydrodynamic approach to dissolution rate. *Pharm. Weekbl.* 3:1005–1020.

Grisafi, F., Brucato, A., Caputo, G., Lima, S. & Scargiali, F., 2023, Modelling particle dissolution in stirred vessels. *Chem. Eng. Res. Des.* 195:662–672.

Hemrajani, R. R. & Tatterson, G. B., 2003, Mechanically Stirred Vessels. *Handbook of Industrial Mixing: Science and Practice* 345–390.

Hirt, C. W. & Nichols, B. D., 1981, Volume of fluid (VOF) method for the dynamics of free boundaries. *J. Comput. Phys.* 39:201–225.

Kaushik, J. K. & Bhat, R., 2003, Why Is Trehalose an Exceptional Protein Stabilizer. An analysis of the thermal stability of proteins in the presence of the compatible osmolyte trehalose. *J. Biol. Chem.* 278:26458–26465.

Kersebaum, J., Flaischlen, S., Hofinger, J. & Wehinger, G. D., 2024, Simulating Stirred Tank Reactor Characteristics with a Lattice Boltzmann CFD Code. *Chem. Eng. Technol.* 47:586–595.

Kolmogorov, A., 1941, Turbulence and Stochastic Process: Kolmogorov's Ideas 50 Years; The Local Structure of Turbulence in Incompressible Viscous Fluid for Very Large Reynolds Numbers (1941). *Proceedings: Mathematical and Physical Sciences* 434:9–13.

Langer, E. & Gillespie, D., 2022,. Report and Survey of Biopharmaceutical Manufacturing Capacity and Production, 19th annual edition. *BioPlan Associates, Inc* 490.

Lasdon, L. S., Fox, R. L. & Ratner, M. W., 1974, Nonlinear optimization using the generalized reduced gradient method. *Rev. française d'Autom., Inform., Rech. opérationnelle Rech. opérationnelle* 8:73–103.

Leslie, S. B., Israeli, E., Lighthart, B., Crowe, J. H. & Crowe, L. M., 1995, Trehalose and sucrose protect both membranes and proteins in intact bacteria during drying. *Appl. Environ. Microbiol.* 61:3592–3597.

Merten, O.-W., 2015, Advances in cell culture: anchorage dependence. *Philos. Trans. R. Soc. B: Biol. Sci.* 370

Mishra, P. & Ein-Mozaffari, F., 2020, Critical review of different aspects of liquid-solid mixing operations. *Rev. Chem. Eng.* 36:555–592.

Murthy, B. N. & Joshi, J. B., 2008, Assessment of standard k–ε, RSM and LES turbulence models in a baffled stirred vessel agitated by various impeller designs. *Chem. Eng. Sci.* 63:5468–5495.

Naumann, Z. & Schiller, L., 1935, A drag coefficient correlation. *Z. Ver. Deutsch. Ing* 77:323.

Neau, H., Pigou M., Fede P., Ansart R., Baudry C., Merigoux N., Lavieville J., Fournier Y., Renon N., Simonin O., 2020, Massively parallel numerical simulation using up to 36,000 CPU cores of an industrial-scale

polydispersed reactive pressurized fluidized bed with a mesh of one billion cells. *Powder Technol.* 366:906–924.

Paul, E. L., Atiemo-Obeng, V. A. & Kresta, S. M., 2003, Handbook of Industrial Mixing.

Pohar, A., 2020, A Review of Computational Fluid Dynamics (CFD) Simulations of Mixing in the Pharmaceutical Industry. *Biomed. J. Sci. Tech. Res.* 27.

Pollard, A. J. & Bijker, E. M., 2021, A guide to vaccinology: from basic principles to new developments. *Nat. Rev. Immunol.* 21:83–100.

Pordal, H. S., Matice, C. J. & Fry, T. J., 2022, The Role of Computational Fluid Dynamics in the Pharmaceutical Industry. *Pharmaceutical Technology*.

Ranz, W. & Marshall, J., 1952, Evaporation from drops. *Chemical Engineering Progress* 48:173–180.

Richards, A. B., 2002, Trehalose: a review of properties, history of use and human tolerance, and results of multiple safety studies. *Food Chem. Toxicol.* 40:871–898.

Rowe, R. C., Sheskey, P. & Quinn, M., 2009, *Handbook of pharmaceutical excipients*.

Sanofi, 2020, Sanofi's Evolutive Vaccine Facility (EVF), Neuville-sur-Saône, France. *Pharmaceutical Technology*.

Shukla, A. A. & Gottschalk, U., 2013, Single-use disposable technologies for biopharmaceutical manufacturing. *Trends Biotechnol.* 31:147–154.

Simonin, O., 1991, Prediction of the dispersed phase turbulence in particle-laden jets. *Gas-Solid Flows ASME* 121.

Smagorinsky, J., 1963, General Circulation Experiments With The Primitive Equations. *Mon. Weather Rev.* 91:99–164.

Sommer, A.-E., Rox, H., Shi, P., Eckert, K. & Rzehak, R., 2021, Solid-liquid flow in stirred tanks: "CFD-grade" experimental investigation. *Chem. Eng. Sci.* 245.

Shu, S. & Yang, N., 2018, GPU-accelerated large eddy simulation of stirred tanks. *Chem. Eng. Sci.* 181:132–145.

Thomas, J. A., 2021, Computational Fluid Dynamics in Upstream Biopharma Manufacturing Processes. *Pharmaceutical Technology* 45:34–40.

Wickramasighe, S. R., Namila, Fan, R. & Qian, X., 2019, Current Trends and Future Developments on (Bio-) Membranes. 69–96.

Yancey, P. H., 2005, Organic osmolytes as compatible, metabolic and counteracting cytoprotectants in high osmolarity and other stresses. *J. Exp. Biol.* 208:2819–2830.